Population Shape Collapse in Large Deformation Registration of MR Brain Images

Wei Shao, Gary E. Christensen, Hans J. Johnson and Joo H. Song
Department of Electrical and Computer Engineering, University of Iowa, Iowa City, IA, USA
{wei-shao, gary-christensen, hans-johnson, joohyun-song}@uiowa.edu,

Oguz C. Durumeric
Department of Mathematics, University of Iowa, Iowa City, IA, USA
oguz-durumeric@uiowa.edu

Casey P. Johnson, Joseph J. Shaffer and Vincent A. Magnotta
Department of Radiology, University of Iowa, Iowa City, IA, USA
{casey-johnson, joseph-shaffer, vincent-magnotta}@uiowa.edu,

Jess G. Fiedorowicz and John A. Wemmie
Department of Psychiatry, University of Iowa, Iowa City, IA, USA
{jess-fiedorowicz, john-wemmie}@uiowa.edu

Abstract

This paper examines the shape collapse problem that occurs when registering a pair of images or a population of images of the brain to a reference (target) image coordinate system using diffeomorphic image registration. Shape collapse occurs when a foreground or background structure in an image with non-zero volume is transformed into a set of zero or near zero volume as measured on a discrete voxel lattice in the target image coordinate system. Shape collapse may occur during image registration when the moving image has a structure that is either missing or does not sufficiently overlap the corresponding structure in the target image[4]. Such a problem is common in image registration algorithms with large degrees of freedom such as many diffeomorphic image registration algorithms. Shape collapse is a concern when mapping functional data. For example, loss of signal may occur when mapping functional data such as fMRI, PET, SPECT using a transformation with a shape collapse if the functional signal occurs at the collapse region. This paper proposes an novel shape collapse measurement algorithm to detect the regions of shape collapse after image registration in pairwise registration. We further compute the shape collapse for a population of pairwise transformations such as occurs when registering many images to a common atlas coordinate system. Experiments are presented using the SyN diffeomorphic image registration algorithm. We demonstrate how changing the input parameters to the SyN registration algorithm can mitigate some of the collapse image registration artifacts.

Keywords: *shape collapse, diffeomorphic image registration*

1. Introduction

Image registration is the process of finding a transformation that defines an optimal pointwise correspondence between a moving image and a target image. The transformation deforms the moving image into the shape of the target image.

Durumeric et al.[4] were the first to investigated the shape collapse problem in nonrigid image registration. Shape collapse occurs when a foreground or background structure in an image with non-zero volume is transformed into a set of zero or near zero volume as measured on a discrete voxel lattice in the target image coordinate system. This may be a desirable property if the structure does not exist in the target image, i.e., no correspondence exists if a structure is present in the moving image but does not exist in the target image. However, a collapse is not desirable if a structure or part of a structure with non-zero volume present in the moving image is mapped to a set of zero volume measured on a discrete voxel lattice rather than to its

corresponding location in the target image. In the later case, the estimated transformation defines an inaccurate point-wise correspondence between the moving and target image. Inaccurate correspondence is a problem when one wants to map information from the coordinate system of the moving image to the coordinate system of the target image. For example, it is common to use the correspondence transformation to map object names/labels or functional data such as fMRI, PET, and SPECT from one image coordinate system to another.

The shape collapse problem is illustrated in Fig. 1 for image registration of two MR images of the brain. Two 3D T1-weighed MR images of the brain were registered using the symmetric diffeomorphic image (SyN) registration [1] method developed by B.B. Avants *et al.* and is distributed as part of the Automatic Normalization Toolkit (ANTs)[2]. In this example, the T1 image shown in Fig. 1a was registered to the image shown in Fig. 1b. Figs. 1c and 1d show the resulting deformed moving images. The red circles show regions of shape collapse. Notice that the cerebral cortex inside the red circles in the deformed image appear to have collapsed in order to match the target image in these regions. Small regions of shape collapse like these are often hard to detect and are often over looked. However, if this transformation is used to map information from the moving image coordinate system to that of the target image, any information such as structure labels or functional brain response would map to a much smaller region in the target coordinate system. It is even possible that all information could be lost if an entire region of interest in the moving image of non-zero volume is mapped to a region of zero volume measured on a discrete voxel lattice in the target image coordinate system. Another problem with transformations that contain regions of shape collapse is that they produce incorrect correspondences in the vicinity of the shape collapse.

We note that shape collapse image registration artifacts like those shown in Fig. 1 are produced by many diffeomorphic image registration algorithms. We chose to study the SyN registration algorithm in this paper since it is publicly available and because it is used in the BRAINS AutoWorkup pipeline (Brain Research: Analysis of Images, Networks, and systems [7]) that is commonly used to non-rigidly register brain images.

We use the simple 2D brain cortex phantoms shown in Fig. 2 to illustrate one type of shape collapse that may occur using common diffeomorphic image registration algorithms. The white object in these phantoms corresponds to a simplified cortex shape in the transverse orientation. The cortex in the moving and target images has a single sulcus. The cortex in the moving image does not fully overlap with the cortex in the target image. When using symmetric diffeomorphic registration with normalized cross correlation

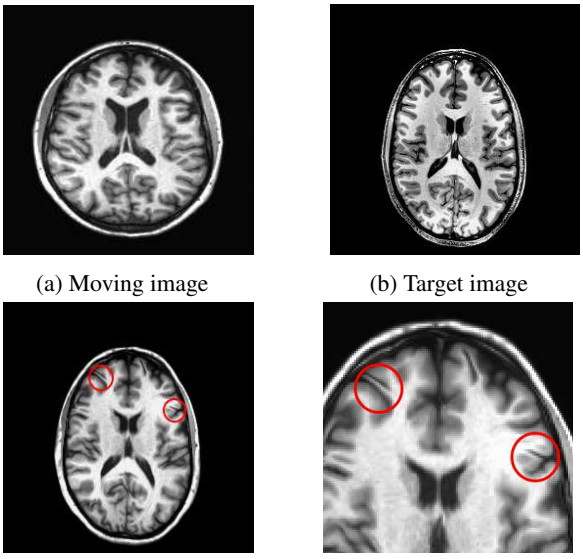

(a) Moving image (b) Target image

(c) Deformed moving image (d) Collapsed regions

Figure 1: Demonstration of shape collapse problem in pairwise 3D MR brain image registration. Panel: a. Transverse slice of moving image, b. Transverse slice of the target image, c. Deformed moving image, collapse regions shown inside red circles, d. Closer view of panel c.

similarity cost function, the non-overlapped cortex in the moving image collapsed to a set of zero volume measured on the discrete voxel lattice and a new cortex grew out of to match the non-overlapped cortex in the target image (see Fig. 2e). The desired transformation to match the moving image with the target image is a local rotation of the cortex in the moving image. The reason why the shape collapse problem exists in the above case is that the similarity cost reduces immediately when the non-overlapped cortex collapses or grows out instead of rotating when using greedy cost function. Therefore, shape collapse is a common problem for image registration methods using greedy cost functions.

The BRAINS AutoWorkup (BAW)[7], is a NiPype (Neuroimaging in Python Pipelines and Interfaces) based workflow that provides an automated procedure for large-scale multi-center longitudinal MR image analysis; this includes denoising, spatial normalization, intra-subject alignment, tissue classification, bias-field correction, and structure segmentation.

In this paper, we investigate the shape collapse problem in MR brain image registration using BRAINS AutoWorkup pipeline, for which symmetric diffeomorphic image registration is part of its image registration process. We also propose an algorithm to detect and measure the shape collapse after image registration. By running shape collapse measurement for each of 50 participants, we obtained a pop-

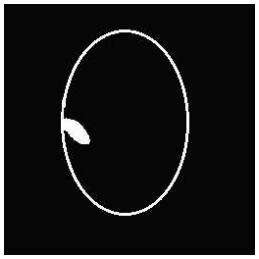

(a) Moving phantom image

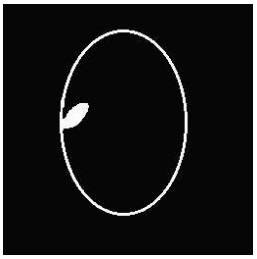

(b) Target phantom image

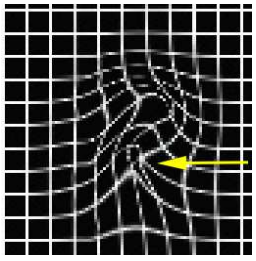

(c) Final deformed grid; zoomed on ROI

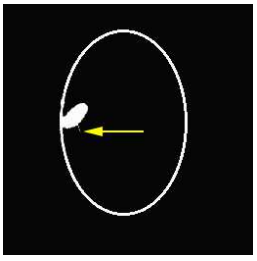

(d) Deformed moving image

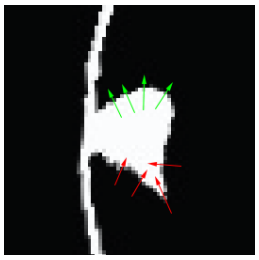

(e) Intermediate deformed moving image; zoomed on ROI

(f) Final deformed moving image; zoomed on ROI

Figure 2: A simple 2D cortex phantom example to explain shape collapse when using diffeomorphic image registration. The cortex in this example has a single sulcus which we will call the region of interest (ROI). Notice that panels b and d look similar and do not appear to have a collapse. Zooming in on the ROI in panels e and f show that sulcus in the moving image did not rotate to match the target sulcus, but rather it compressed (collapsed) at the bottom and grew from the top. A small collapse artifact that is often over looked or ignored can be seen in panel f at the bottom part of the deformed sulcus. The deformed grid shows the collapse. Red arrows in the intermediate deformed moving image shows the direction of cortex in the moving image collapsed and green arrows indicate the direction of new cortex grew out (i.e., the background collapsed to a set of zero volume measured on the discrete voxel lattice) to match the reference image.

ulation probability map of shape collapse to predict regions that are more likely to collapse when using deformable image registration.

2. Methods

2.1. SyN, Symmetric Diffeomorphic Image Registration

The SyN symmetric diffeomorphic image registration algorithm [1] registers two images by mapping each image to a midpoint coordinate system. Let $I_0 : \Omega \to \mathbb{R}$ and $I_1 : \Omega \to \mathbb{R}$ represent two images to be registered where $\Omega \subset \mathbb{R}^n$ is the domain of the images. Define $\phi_0 : \Omega \times [0,1] \to \Omega$ to be a homotopy between the functions $\phi_0(\cdot,0) = f$ and $\phi_0(\cdot,1) = g$ such that $f = Id$ is the identity map and g is the mapping that deforms I_0 into the shape of I_1 via the action $g \cdot I_0 \triangleq I_0(g^{-1})$. Define $\phi_1 : \Omega \times [0,1] \to \Omega$ similarly such that $\phi_1(\cdot,0) = Id$ and $\phi_1(\cdot,1) \cdot I_1 = I_1(\phi_1^{-1}(\cdot,1))$ maps I_1 into the shape of I_0. Let $v : [0,1] \to V$ be a time-dependent velocity vector field where V is a Hilbert space of smooth, compactly supported vector fields on Ω. The diffeomorphic properties of the transformation ϕ_0 and ϕ_1 comes from the fact that each is constrained to satisfy the O.D.E $\frac{d}{dt}\phi_i(x,t) = v_i(\phi_i(x,t),t)$ for $i = \{0,1\}$, $t \in [0,1]$, $x \in \Omega$, and the velocity fields $v_i \in L^2([0,1],V)$[3].

The SyN registration algorithm is stated as: Minimize the following cost function with respect to v_0 and v_1

$$E(v_0,v_1) = \int_0^{0.5} \Big\{ ||v_0(x,t)||_V^2 + ||v_1(x,t)||_V^2 \Big\} dt + \int_\Omega CC\big(I_0(\phi_0^{-1}(x,0.5)), I_1(\phi_1^{-1}(x,0.5))\big) dx \tag{1}$$

where $CC(\cdot,\cdot)$ is the normalized cross correlation and $||v(x,t)||_V$ is a Sobolev norm on the velocity field. Notice that the normalized cross correlation is computed in a mid-point coordinate system that is half-way between the coordinate systems of I_0 and I_1, i.e., in the $t = 0.5$ coordinate system.

Following the notation of [1], the normalized cross correlation is defined in the following way. Define the images with their local mean subtracted as $\bar{I}(x) = I_0(\phi_0^{-1}(x,0.5)) - \mu_{I_0}(x)$ and $\bar{J}(x) = I_1(\phi_1^{-1}(x,0.5)) - \mu_{I_1}(x)$ where μ_{I_i} is the the local mean of the intensity centered at x in a $5 \times 5 \times 5$ window. The normalized cross correlation is then defined as

$$CC(\bar{I},\bar{J}) = \frac{< \bar{I},\bar{J} >^2}{< \bar{I} >< \bar{J} >} = \frac{A^2}{BC} \tag{2}$$

where the inner products are taken over a $5 \times 5 \times 5$ window.

The inner-product of two vector fields in the vector space V is defined through a differential operator L given by:

$$< f,g >_V \triangleq < Lf, Lg >_{L^2} = < L^+Lf, g >_{L^2} \tag{3}$$

where L^+ is the adjoint of operator L.

From the above construction of the vector space V, a compact self-adjoint operator [3] $K : L^2(\Omega, \mathbb{R}) \rightarrow V$ is uniquely defined by

$$< a, b >_{L^2} = < Ka, b >_V \quad (4)$$

The operator K is a Gaussian filter in the implementation of SyN algorithm in ITK.

Following the derivations in Beg et al.[3] and Avants et al. [1], the gradients of the energy functional with respect to $v_1(t)$ and $v_1(t)$ are given as

$$\nabla_{v_0} E = 2v_0(x,t) + K\Bigg(\frac{2A}{BC} \times \Big(\bar{J}(x) - \frac{A}{B}\bar{I}(x)\Big)|D\phi_0(x, 0.5)|\nabla\bar{I}(x)\Bigg) \quad (5)$$

$$\nabla_{v_1} E = 2v_1(x,t) + K\Bigg(\frac{2A}{BC} \times \Big(\bar{I}(x) - \frac{A}{C}\bar{J}(x)\Big)|D\phi_1(x, 0.5)|\nabla\bar{J}(x)\Bigg) \quad (6)$$

2.2. Collapse Detection

Let Ω_0 and Ω_1 be two differentiable manifolds that represent the domains of images $I_0 : \Omega_0 \rightarrow \mathbb{R}$ and $I_1 : \Omega_1 \rightarrow \mathbb{R}$, respectively. Define the transformation $\varphi : \Omega_0 \rightarrow \Omega_1$ to be the transformation that acts on I_0 to transform it into the shape of I_1 via the action $\varphi \cdot I_0 \triangleq I_0(\varphi^{-1})$. Note that $\varphi^{-1} : \Omega_1 \rightarrow \Omega_0$ is a mapping from the domain of I_1 to the domain of I_0. We say that a collapse happens at $y \in \Omega_0$ when φ maps an open set $U \subset \Omega_0$ containing y to an open set $\varphi(U) \subset \Omega_1$ of near zero measure. Alternatively, we say a collapse happens at $x \in \Omega_1$ if there exists an open (round) ball $V \in \Omega_1$ containing x such that $\varphi^{-1}(V)$ is mapped to an almost disconnected set (concentrated in at least two different regions joined by thin connectors, such as an hourglass) in Ω_0.

Theoretically, shape collapse occurs in regions of near zero Jacobian determinant with respect to the push forward transformation φ. But in practice we will not use Jacobian determinant as a measure of shape collapse for two main reasons: (1) We do not have access to the vector field at each time point from the SyN algorithm; (2) If we could calculate the Jacobian in the continuum, we would still have the problem that the region of points of near zero Jacobian determinant would be a thin region in between the voxel lattice samples in the fixed image coordinate system. Thus, we can not calculate the Jacobian on the discrete lattice of the fixed image coordinate system.

The second definition of shape collapse above is more convenient for detecting points of collapse in image registration since φ^{-1} is used to compute the deformed image of I_0 into the shape of I_1. In the case of the SyN registration algorithm, we define $\varphi^{-1} \triangleq \phi_0^{-1}(\cdot, 0.5) \circ \phi_1(\cdot, 0.5)$ and $\Omega_0 = \Omega_1 = \Omega$ to be consistent with Eq. 1.

The following algorithm is used to detect where points of collapse occur in the domain Ω_1 of the image I_1. Let $G_1 \subset \Omega_1$ denote the discrete collection of voxel center locations corresponding to the centers of the voxels of image I_1. Repeat the following steps for each $x \in G_1$.

1. Let $N_x \subset G_1$ be a neighborhood of x.
2. Let $D_x = \{\varphi^{-1}(y) - y | y \in N_x\}$ be the set of displacement vectors in the neighborhood of x.
3. Compute the 2-means clustering of the set D_x. Let μ_1 and μ_2 denote the values of the two means, respectively.
4. Let $d_x = ||\mu_1 - \mu_2||$ denote the Euclidean distance between the two means.

Form the image of collapse points $C : \Omega_1 \rightarrow \mathbb{R}$ using the rule $C(x) = d_x$ for $x \in G_1$.

The results in this paper used a 3×3 voxel neighborhood for the 2D results and a $3 \times 3 \times 3$ voxel neighborhood for the 3D results.

3. Experiments and results

3.1. Imaging data

Anatomical images from a study of bipolar disorder were used in this analysis including images from 25 participants with bipolar disorder (14 male: 11 female; age m = 38.6, sd = 13.06) and 25 healthy control participants (14 male: 11 female; age m = 38.36, sd = 13.23). Participants provided written informed consent prior to participation in the study. T1-weighted images were acquired with 1mm^3 isotropic resolution using a 3T Siemens scanner. T1-weighted images were acquired using a 3D magnetization-prepared rapid gradient echo sequence in the coronal plane (FOV: 256x256x256 mm^3; matrix = 256x256x256, TR=2530ms; TE = 2.3ms; TI = 909ms; flip angle = 10; bandwidth = 180 Hz/pixel; and R=2 GRAPPA).

3.2. Image Registration Using BRAINS AutoWorkup

BRAINS AutoWorkup [7] provides a framework for automatically analyzing MRI scans that incorporates several steps to provide well defined mappings between each subject scan and a common brain atlas (NAC HNCMA Atlas 2013 [6]). First, the anterior commissure (AC) point, posterior commissure (PC) point and 49 other fiducial points are automatically detected by the BRAINS Constellation Detector [5] for both the atlas and the subject images. A rigid transformation for each data set is computed that aligns the

AC point to (0,0,0) and sets the PC point to (0,−|AC-PC|,0), and the mid-sagittal plane (MSP) is identified by optimizing the plane that maximally correlates intensity values from the right hemisphere to the left hemisphere (as if reflected in a mirror). The rigid transformation is incorporated into the physical space definition of image headers to avoid introducing interpolation errors. This results in both the atlas and the subject being aligned at the AC point, along the AC-PC line, and within the MSP. Subsequent to this initialization phase, the previously identified 51 landmark points in atlas and subject space are used to estimate an affine transform used to initialize the symmetric diffeomorphic image registration. In this work, we use the inverse transformation estimated from BAW to register T1 AC-PC aligned image to the common atlas space.

3.3. Shape collapse measurement results

By computing the Euclidean distance d_x for each point x in the atlas space, we can generate a shape collapse map for each participant. Fig. 3 is a shape collapse map for one of the 50 participants. In this example, we use a color overlay to visualize areas where our algorithm detected shape collapse (red regions in Fig. 3b). These regions are consistent with the areas where shape collapse was visually apparent in the deformed image (Fig. 3a), confirming that our algorithm has successfully detected regions where shape collapse occurred during image registration.

3.4. Population Shape-Collapse Probability Map

The shape collapse algorithm was used to compute the shape collapse maps for all of the 50 participants (25 healthy controls and 25 people with bipolar disorder). For each participant, a universal threshold T was applied to the corresponding map of shape collapse, and the average of all the 50 thresholded maps gives a population shape-collapse probability map for the whole brain. Let $C_i : \Omega_r \rightarrow \mathbb{R}$ denote the map of shape collapse measurement for the ith subject, where Ω_r is the domain of reference image. Let $Prob : \Omega_r \rightarrow \mathbb{R}$ denote the population probability map of shape collapse, for any point $p \in \Omega_r$ we have

$$Prob(p) = \frac{1}{50} \sum_{i=1}^{50} Thres(C_i(p))) \tag{7}$$

where $Thres : \mathbb{R} \rightarrow \{0, 1\}$ is a function defined as $Thres(a) = 0$ if $a < T$, and $Thres(a) = 1$ if $a \geq T$. The probability map of shape collapse across 50 subjects is shown in Fig. 4.

The population, shape-collapse, probability map gives information about the regions where shape collapse problem is more likely to occur for this population during diffeomorphic image registration. This information can be used to determine whether or not there is functional signal loss when mapping functional data to a reference coordinate system, develop algorithmic solutions to reduce shape collapse problems and to determine the validity of population shape measurements when using nonrigid image registration methods.

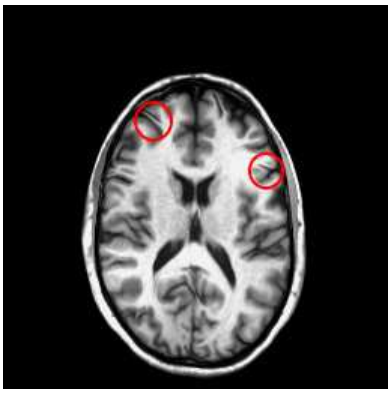

(a) Deformed T1 image

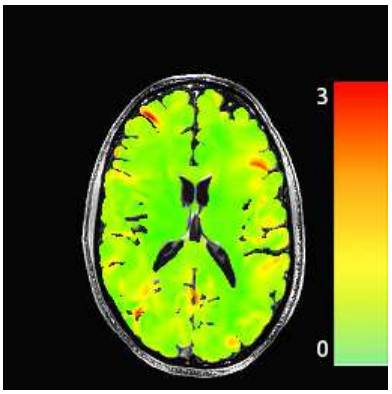

(b) Collapse measurement

Figure 3: Shape collapse detection for one participant. (a) same deformed image as in Fig. 1c; (b) color coded collapse image superimposed on image shown in (a) where green corresponds to a collapse value of 0 mm and to red corresponds to a collapse value of 3 mm. Red regions are regions with shape collapse after registration.

3.5. Gaussian Smoothing Kernel Analysis

We investigated the influence of the Gaussian smoothing kernel K (see Eq. 4) for the SyN registration algorithm using the 2D moving and target phantom images shown in Fig. 2. The SyN registration algorithm was used to register the moving brain phantom to the target brain phantom using a Gaussian smoothing kernel with different variances σ^2. Results of these experiments are shown in Fig. 5. Notice that there is more shape collapse for smaller sigmas than for larger sigmas in this figure.

Table 1 shows the sum of squared differences between the deformed moving image and the target image for var-

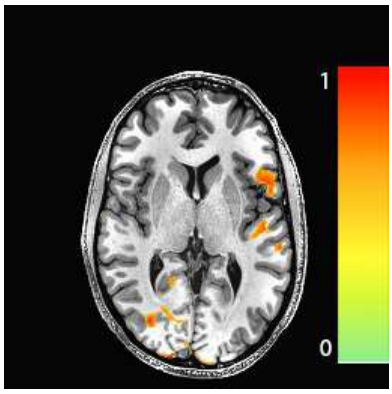

(a) Axial view

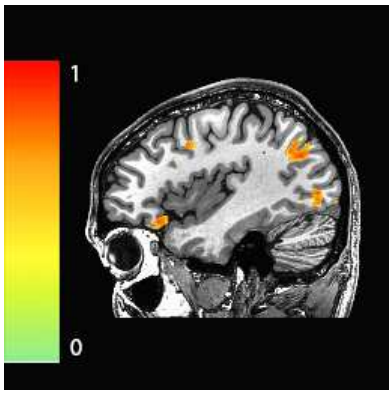

(b) Sagittal view

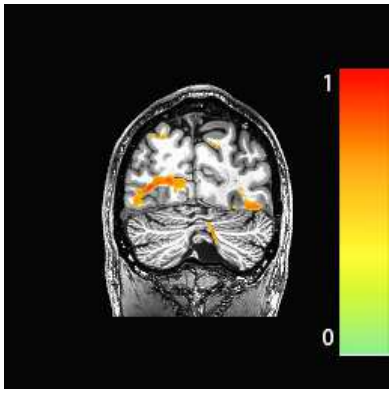

(c) coronal view

Figure 4: Orthogonal views of the 3D population, shape-collapse, probability map in the atlas space (includes 25 normal controls and 25 euthymic individuals). The probability map was obtained with threshold value $T = 1$ (i.e., the threshold value of the $Thres$ function in Eq. 7 was set to 1). This population, shape-collapse, probability maps was thresholded at 0.6 (i.e., regions with value less than 0.6 mm are not visualized). Regions of red and orange show areas of collapse that occur across at least 60% of the individuals in the population.

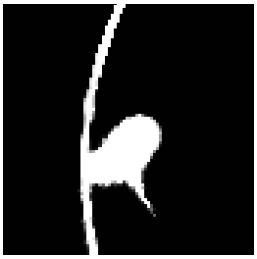

(a) Deformed image, $\sigma^2 = 1$

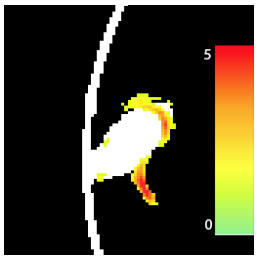

(b) Collapse map, $\sigma^2 = 1$

(c) Deformed image, $\sigma^2 = 1.5$

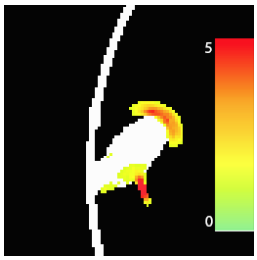

(d) Collapse map, $\sigma^2 = 1.5$

(e) Deformed image, $\sigma^2 = 2$

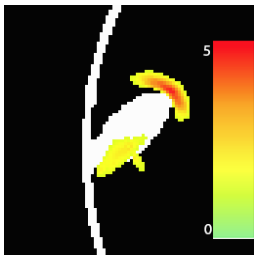

(f) Collapse map, $\sigma^2 = 2$

Figure 5: Registration results for three SyN registrations that registered the moving and target images shown in Fig. 2. The variance σ^2 of the Gaussian smoothing kernel used for registration is shown under each panel. Each collapse map was thresholded at a value of 2.0 mm for better visualization. Notice that more collapse happens using a kernel with a smaller variance than with a larger variance.

ious Gaussian smoothing kernels. This table shows that when smooth variance is very small, the shape collapse is small but the registration result is not desirable, i.e., there is a large sum of squares intensity difference between the deformed moving image and the target image. As the variance increases, the shape collapse increases and the registration result is getting better. But when variance becomes too large (i.e., variance = 3), the shape collapse still goes down, but the registration result gets worse. This shows that there is a trade-off between the amount of shape collapse and the accuracy of the registration result.

Variance, σ^2	Collapse$_{mean}$	Collapse$_{max}$	Sqrt(SSD)
0.5	1.57	3.48	3627
1.0	1.70	5.25	2597
1.5	1.71	6.24	1544
2	1.66	4.90	1152
2.5	1.58	3.01	1293
3	1.55	3.17	1180
3.5	1.54	3.06	1245
4	1.53	2.97	1606

Table 1: Results of SyN registration with different smoothing kernels. The first column shows the different smoothing variances used for the Gaussian smoothing kernel. The second and third columns show the mean and maximum values of voxels with value greater than 1 mm in the collapse map, respectively. The last column shows the square roots of the sum of squared differences between the deformed moving image and target image.

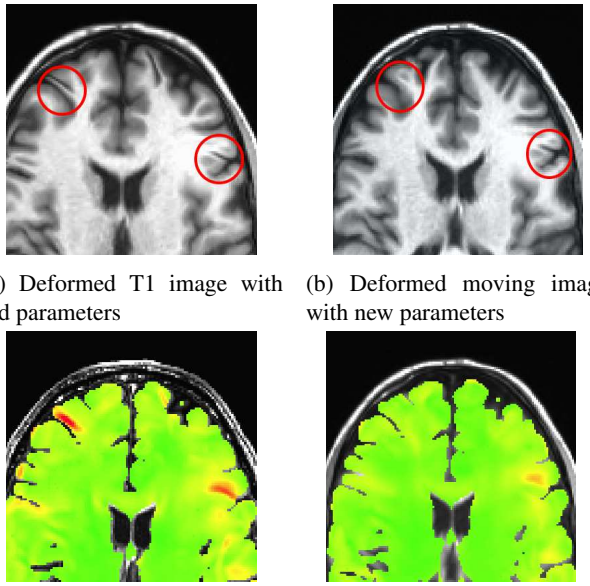

(a) Deformed T1 image with old parameters

(b) Deformed moving image with new parameters

(c) Collapse measurement with old parameters

(d) Collapse measurement with new parameters

Figure 6: Shape collapse map for the same participant shown in Fig 3 when using new BRAINS AutoWorkup. The same color scale is used as in Fig 3 where orange regions are regions with large shape collapse after image registration. Notice that panels c and d show that the shape collapse was dramatically reduced using the new BAW for the same participant.

3.6. Retrospective Comparison of Two Sets of Parameters Used for SyN Registration in BAW

In this section, we discuss a retrospective comparison between two sets of parameters used for SyN image registration using the BRAINS AutoWorkup (BAW). The SyN registration parameters used in the BAW pipeline are hard coded in the scripts. We noticed some collapse registration artifacts in registration results generated two years ago using BAW that appeared to disappear or become less noticeable using a newer version of the BAW. Figure 3 shows the collapse artifacts for one participant using the old BAW and Fig. 6 shows the corresponding collapse map using the new parameters for the same participant. Figure 7 shows the population shape-collapse probability map using the results from the new BAW. Comparing Figs. 3 and 7 shows that the overall probability of shape collapse for the population was substantially reduced during registration using the new BAW.

When we investigated what was different between the old and new BAW, we found that the variance of the Gaussian kernel K in Eq. 4 used to smooth the update velocity field at each iteration stayed the same between the two sets of parameters. The gradient step size decreased by 50% in the new BAW compared to the old BAW. This change makes the convergence of the gradient descent of the new method slower, but, should not contribute to image collapse registration artifacts.

This meant that the main difference between the old and new SyN registration parameters was the multi-resolution scheme used to estimate the transformation. The old version of BAW uses a four level multi-resolution scheme for optimization while the new BAW uses multi-stage, multi-resolution registration scheme with two stages and two levels for each stage. In the old scheme, the two images are down sampled by 5, 4, 2, 1 (full resolution) and registered for 10000, 500, 500, and 200 iterations or until convergence at each resolution, respectively. In the new scheme, the two images are down sampled by 8 and 4 and registered for 500 and 500 at each resolution or until convergence in the first stage, respectively. Incorporating the results from the first stage, the two images are down sampled by 2 and 1 (full resolution) and registered for 500 and 70 at each resolution or until convergence in the second stage, respectively.

Table 2 shows that although the shape collapse was mitigated with the new SyN parameters, the registration results got worse as measured by the normalized cross correlation. This table suggests that the reason that the new SyN registration parameters produce less shape collapse is because the algorithm stops before convergence at the full image resolution. Allowing the SyN image registration algorithm to iterate more than 70 iterations at the full image resolution would result in a reduction in the normalize cross correlation and an increase in shape collapse. This shows that one has to find a balance between the amount of image registration accuracy and the amount of shape collapse.

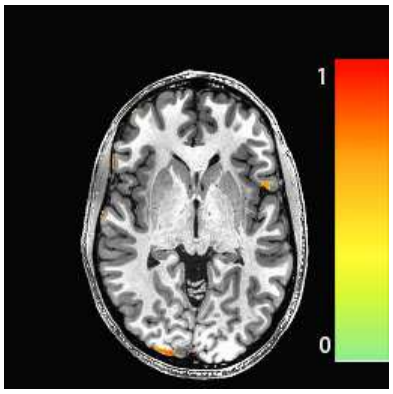

(a) Axial view

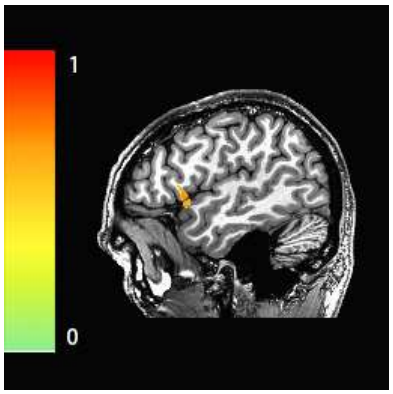

(b) Sagittal view

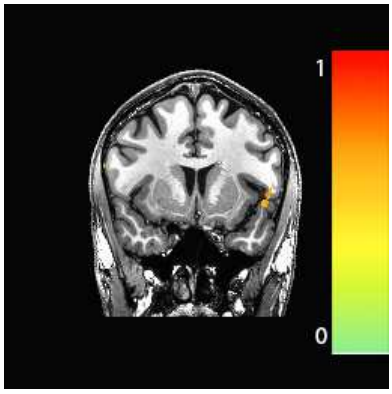

(c) coronal view

Figure 7: Orthogonal views of the 3D population, shape-collapse, probability map in the atlas space using new BRAINS AutoWorkup. The probability map is obtained with threshold value 1 (sets threshold value T of function $Thres$ in Eq. 7 to 1). And three views are thresholded at 0.6 (regions with value less than 0.6 mm will not show up). Regions of red and orange show areas of collapse that occur across at least 60% of the individuals in the population.

ID	CC_{old}	CC_{new}	$Collapse_{old}$	$Collapse_{new}$
1	0.63	0.57	3.91	2.88
2	0.63	0.56	4.25	2.47
3	0.62	0.54	4.19	3.63
4	0.66	0.58	3.87	2.37
5	0.66	0.59	4.47	3.04
6	0.64	0.59	3.84	2.69

Table 2: Summary statistics for six participants chosen randomly from the population for the old and new SyN registration parameters. The largest value of shape collapse using the old and new parameters for these participants are shown in the forth and fifth columns, respectively. For each participant, the normalized cross correlation between the deformed and reference images using the old (CC_{old}) and new (CC_{new}) SyN registration parameters is shown in the second and third columns, respectively.

4. Summary and Conclusions

We presented a new method to detect shape collapse in pairwise nonrigid image registration. We extended this algorithm to compute the population, shape-collapse probability map. This map can be used to determine whether or not there is functional signal loss when mapping functional data to a reference coordinate system, develop algorithmic solutions to reduce shape collapse problems and to determine the validity of population shape measurements when using nonrigid image registration methods.

5. Acknowledgments

This study was supported by the generous donation provided by a Roger Koch. Archive and storage of imaging data was supported by the University of Iowa Institute for Clinical and Transnational Science (U54TR001013).

J.A.W. was supported by the Department of Veterans Affairs (Merit Award), the NIMH (5R01MH085724), NHLBI (R01HL113863) and a NARSAD Independent Investigator Award. J.G.F. was supported by the NIMH (K23MK083695) and NHLBI (P01HL014388). V.A.M was supported in part by a NARSAD independent Investigator Award.

We would like to thank Regina EY Kim and Ali Ghayoor for their help with BRAINS AutoWorkup.

References

[1] B. B. Avants, C. L. Epstein, M. Grossman, and J. C. Gee. Symmetric diffeomorphic image registration with cross-correlation: evaluating automated labeling of elderly and neurodegenerative brain. *Med Image Anal*, 12(1):26–41, Feb 2008.

[2] B. B. Avants, N. J. Tustison, G. Song, P. A. Cook, A. Klein, and J. C. Gee. A reproducible evaluation of ants similarity metric performance in brain image registration. *Neuroimage*, 54(3):2033–2044, 2011.

[3] M. Beg, M. Miller, A. Trouvé, and L. Younes. Computing large deformation metric mappings via geodesic flows of diffeomorphisms. *International Journal of Computer Vision*, 61(2):139–157, 2005.

[4] O. C. Durumeric, I. Oguz, and G. E. Christensen. The shape collapse problem in image registration. In *Mathematical Foundations of Computational Anatomy*, pages 95–106.

[5] A. Ghayoor, J. G. Vaidya, and H. J. Johnson. Development of a novel constellation based landmark detection algorithm. In *SPIE Medical Imaging*, pages 86693F–86693F. International Society for Optics and Photonics, 2013.

[6] M. Halle, I.-F. Talos, M. Jakab, N. Makris, D. Meier, L. Wald, B. Fischl, and R. Kikinis. Multi-modality mri-based atlas of the brain. In *SPL*, 11 2015.

[7] E. Y. Kim and H. J. Johnson. Robust multi-site mr data processing: iterative optimization of bias correction, tissue classification, and registration. *Frontiers in neuroinformatics*, 7(29), 2013.